THE ASTROPHYSICAL JOURNAL, 258:224–235, 1982 July 1

TIME-RESOLVED SPECTROSCOPY OF THE ACCRETION DISK IN RW TAURI

RONALD H. KAITCHUCK[1] AND R. KENT HONEYCUTT[1]
Astronomy Department, Indiana University
Received 1981 October 19; accepted 1982 January 21

ABSTRACT

Time-resolved spectroscopy of the Algol RW Tauri during 12 eclipses has determined the following characteristics of the disk. The disk is smaller than previously believed (rarely exceeding 1.5 times the radius of the central star) and shows significant variations in size in one orbit. The emission-line widths are always at least twice that expected from broadening by rotational motion in a disk. While the nearly Gaussian line profiles suggest turbulence, it would be required to be highly supersonic.

A detailed study of one particularly favorable eclipse shows $\bar{n}_e$ to be approximately 10^{11} cm^{-3}. The trailing side of the disk appears to be nearly isothermal, of approximately constant density, and with an apparent radius that is likely set by the ionization limit. The rotational velocity field is highly non–Keplerian; on the leading side of the disk, the highest rotational velocity is at the *outer* edge. There is additional indirect evidence of infall toward the central star and a collapse toward the orbital plane as the gas moves from the trailing to the leading side.

Subject headings: stars: accretion — stars: eclipsing binaries — stars: individual

I. INTRODUCTION

Accretion disks in close interacting binary stars are a common phenomenon. Disk or ring structures surrounding the mass-gaining star manifest themselves in a variety of ways including excess continuum light and Doppler-shifted emission lines. In deep eclipsing Algol systems, it is sometimes possible to see emission lines during eclipse whose strength and velocity variations have been interpreted for nearly 40 years as evidence for a disklike structure surrounding the primary. This paper examines in detail the nature of the disk in one such Algol.

RW Tauri (BD +27°623) is a well-known Algol-type eclipsing binary system. Every 2.769 days the B8 V primary star is totally eclipsed for 80 minutes by the K0 IV secondary, producing the deepest eclipse known, over 5 mag in the ultraviolet. Wyse (1934) discovered the presence of Doppler-shifted emission lines during totality. Subsequently, Joy (1942) found that the emission lines seen at second contact were displaced redward by about 350 km s^{-1}. Near mid-eclipse the lines disappeared only to reappear near third contact with a blueshift of about 350 km s^{-1}. Unfortunately, Joy could only obtain about three spectrograms each orbit showing the emission lines because the brilliance of the primary star makes them practically undetectable outside of the brief total phase. Joy suggested a model in which the primary star is surrounded by a rotating, gaseous ring. At second contact the side of the ring rotating away from the observer is visible, while at third contact the side rotating toward the observer is seen. The emission lines disappear at mid-eclipse since the ring is totally eclipsed. This basic model has not been significantly refined observationally since Joy's work. It is the earliest model for a class of objects now known as accretion disks.

As the disk undergoes eclipse the emission-line spectrum is expected to evolve rapidly as regions of differing physical conditions and rotational velocities are occulted. Therefore, there is much valuable information to be gained from time-resolved spectroscopy in eclipse. The simultaneous constraints of time resolution sufficient to resolve spatial structure and spectral resolution sufficient to resolve the Doppler shifts demand a modern low-light-level multiplexed detector and an automatic data acquisition system to minimize "dead time" between integrations. We used the SIT vidicon spectrometer at Indiana University's Goethe Link Observatory and the intensified image dissector scanner (I-IDS) spectrometer at Kitt Peak National Observatory (KPNO) to obtain the first successful time-resolved spectroscopy of the disk in the RW Tauri system.

Accretion disks in interacting binaries are now recognized to be the result of Roche lobe overflow. In short-period Algol systems, such as RW Tauri, the stream from the inner Lagrangian point is expected to strike the trailing hemisphere of the primary star. The disk presumably results from the star-stream interaction, although the details of its formation are unknown. In cataclysmic systems and long-period Algol systems, the size of the mass-gaining star is much smaller compared to the stellar separations. In these cases the stream misses the star and forms stable orbits (Lubow and Shu 1975). It is, therefore, expected that the disks in short-period Algol systems will differ from those in cataclysmic

[1] Visiting Astronomer, Kitt Peak National Observatory, which is operated by the Association of Universities for Research in Astronomy, Inc., under contract with the National Science Foundation.

systems and from the "standard" disk models such as those of Shakura and Sunyaev (1973). Nevertheless, these structures are important in their own right and may lead to important insights into the star-stream interaction and the accretion process in general. Algol systems offer some important advantages over cataclysmic systems for this type of study. They lack the complication of a stream impact spot producing additional continuum and line emission, and we have a much better understanding of eclipse geometry, stellar masses, and radii. Furthermore, short-period Algol systems have eclipses of short duration which helps to ensure that the observations represent a "snapshot" of disk structure.

II. OBSERVATIONS

The observations were obtained at Goethe Link Observatory and KPNO. The Link facilities consisted of a 0.91 m telescope equipped with a Meinel spectrograph with an S-20, SIT vidicon detector. The spectrograph was operated in a "time-resolved" mode where the integrations alternated between two digital memories in such a way that each spectrum was recorded on a magnetic diskette after the next integration had begun, resulting in only 2 seconds of "dead time" between integrations due to the target preparation cycle. Most of the observations were made at Hα using a 300 lines mm^{-1} grating blazed at 4200 Å. This gave a resolution of 8 Å and a wavelength coverage of 500 Å. Integration times were typically 300 seconds, which allowed about 15 spectra to be recorded during totality.

The KPNO observations were obtained with the 2.1 m telescope, the gold spectrograph, and the I-IDS. Integration times were 120 seconds with 15–30 seconds between observations for data recording and beam switching between entrance apertures. Approximately 30 spectra were obtained during totality. The observations were made in the Hβ-Hγ region using an 831 lines mm^{-1} grating in second order. The spectral resolution was typically 2.5 Å, and the entrance apertures were circular with diameters of 6″.1. Spectrophotometric standards were observed, and the RW Tauri spectra were transformed to an absolute flux scale.

For a proper interpretation of the observations, it was necessary to establish accurately the time of second and third contact. This is complicated by two problems. The first is the well-known period variations of RW Tauri (see for example, Frieboes-Conde and Herczeg 1973). This was solved by photometrically observing two eclipses in the 1978 and 1979 observing season to establish reliable times of minima for that epoch. For the 1980 and 1981 eclipses the times of minima were computed from a new set of light elements kindly supplied by E. C. Olson:

$$\text{Min I (HJD)} = \underset{\pm 3}{2440127.1490} + \underset{\pm 3}{2.7688409}\ \text{E} .$$

The next problem was to establish the contact points relative to mid-eclipse (i.e., their phases). Unfortunately, excess continuum emission from the disk usually prevents the light curve from being flat-bottomed in totality. This effect was noted by Grant (1959), and its great variability from eclipse to eclipse has been clearly demonstrated by Olson (1980*a*). The phases of the contact points were established in two ways. First, the continuum emission is strongly wavelength dependent. Olson's (1980*a*) photometry shows it to be almost negligible in the red. Therefore, the contact points were estimated from Bookmyer's (1977) *R*-photometry. Second, Olson's (1980*a*) photometry shows the eclipse of 1978 November 8, to be flat-bottomed. Our spectroscopy on that night showed the emission lines to be extremely weak. This light curve was considered to be nearly "undisturbed" and was also used to estimate the contact points. A weighted mean was formed and the adopted phases of second and third contact were 0.9901 ± 0.0002 and 0.0099 ± 0.0002 respectively. An important advantage of the I-IDS system for this type of study is its use of a circular entrance aperture rather than a slit, which allows a light curve to be extracted from the spectroscopic data. This provided a valuable check of the predicted time of minimum light.

In all, 18 eclipses were observed. Emission lines were detected on only 12 occasions, confirming Joy's (1947) finding that the disk is not always present. Table 1 summarizes the observations, indicating the spectral region covered (by the hydrogen lines visible in the bandpass), the spectral and time resolution, and the phase coverage. Columns (6) and (7) indicate if emission lines were detected and give an upper limit to the equivalent width of a null detection. In several cases the emission lines were weak and only detected after co-adding the spectra taken during totality. These cases are noted. Table 2 summarizes just the disk detections. Column (1) contains the UT dates, and column (2) gives the spectral line used to obtain the values in the next four columns. In order to compare line strengths among eclipses, column (3) gives the equivalent width of the emission line at second contact. Columns (4) and (5) contain the full width at half-maximum of the emission line at second and third contact, respectively, corrected for instrumental resolution. Note that the line widths at the two contact points are always the same to within observational error, and the line widths are very large, ranging from 230 to over 600 km s^{-1}. Column (6) contains the ratio of the line strengths at second and third contact. The strength of the redshifted component is always equal to, or greater than, the strength of the blueshifted component.

The last two columns contain the disk radius on the trailing (redshifted) and leading (blueshifted) side of the primary star. The disk radii were determined in the following manner. The duration of totality in phase units is 0.0198. During this interval, as seen from the Earth, the B star moves (relative to the K star) a distance equal to the difference in diameter of the two stars. Grant's (1959) light curve solution gives the ratio of stellar radii as 0.748. The difference in their diameters is $2[(1/0.748) - 1]\ R_*$, where R_* is the radius of the primary star. The "velocity" of the star in units of radii per unit phase is $2\ R_*[(1/0.748) - 1]/0.0198 = 34.030\ R_*$.

TABLE 1

SUMMARY OF RW TAURI OBSERVATIONS

UT Date (1)	Spectral Region (2)	Spectral Resolution (Å) (3)	Time Resolution (s) (4)	Phase Coverage (5)	Emission Detected? (6)	Comments (7)
1978 Feb 7.....	Hα	8.6	400	0.97–0.03	yes	emission strength peaked after second contact
Sep 8	Hα	10.2	400	0.00–0.02	yes	co-adding required
Oct 25	Hα	8.3	400	0.97–0.00	yes	co-adding required
Oct 28	Hα	8.9	400	0.98–0.02	no	EW < 0.3 Å
Nov 8	Hα	8.4	400	0.96–0.02	yes	co-adding required
Nov 19.....	Hα	11.2	400	0.99–0.02	yes	co-adding required
Dec 28	Hα	8.8	300	0.99–0.01	yes	very strong
1979 Feb 2.....	Hα	4.4	500	0.97–0.00	yes	strong
Nov 3	Hα	8.0	300	0.99–0.02	no	EW < 1.3 Å
Nov 17.....	Hα	8.0	300	0.00–0.04	no	EW < 1.0 Å
Nov 25.....	Hβ–Hγ	2.5	120	0.98–0.02	yes	moderately strong
Nov 28.....	Hβ–Hγ	2.5	120	0.99–0.02	yes	strong
Dec 20	Hβ–Hε	8.0	300	0.96–0.01	no	EW < 1.2 Å
1980 Oct 3.....	Hα	7.3	400	0.97–0.01	no	EW < 4.5 Å
Nov 30.....	Hα	11.2	300	0.96–0.00	no	EW < 1.2 Å
Dec 14	Hβ–Hε	9.7	300	0.96–0.02	yes	very strong
1981 Jan 8	Hβ–Hε	8.4	300	0.98–0.01	yes	moderately strong
Feb 24	Hβ–Hγ	2.7	120	0.98–0.02	yes	strong

If the redshifted side of the disk is completely covered, and hence the emission disappears by phase, t_r, then the disk radius on the trailing side, r_r, is

$$r_r = [34.030(t_r - 0.9901) + 1]\, R_* \,. \quad (1)$$

A similar expression holds for the blueshifted side, namely,

$$r_b = [34.030(0.0099 - t_b) + 1]\, R_* \,, \quad (2)$$

where t_b is the phase at which the blueshifted emission is first detected.

The disk radii in Table 2 were calculated from these two equations. To express these radii in terms of the stellar separation, multiply by 0.185 (Grant 1959). In only seven cases were the emission lines strong enough to allow a reliable estimate of t_r and t_b. The disk radii are all surprisingly small. Values of 2–3 times the B star radius have been quoted in the past by Batten (1973)

TABLE 2

SUMMARY OF RW TAURI DISK DETECTIONS

UT Date (1)	Line (2)	EW at Second Contact (Å) (3)	FWHM at Second Contact (km s^{-1}) (4)	FWHM at Third Contact (km s^{-1}) (5)	I_r/I_b at Contacts (6)	Radius Trailing (r_r/R_*) (7)	Radius Leading (r_b/R_*) (8)
1978 Feb 7.....	Hα	11.5[a]	480 ± 100	490 ± 10	~1	1.4 ± 0.1	1.2 ± 0.1
Sep 8.....	Hα	~3.8[b]	~300	~300	[c]	[c]	[c]
Oct 25.....	Hα	~0.7[b]	<380	<380	[c]	[c]	[c]
Nov 8	Hα	~1.2[b]	<380	<380	[c]	[c]	[c]
Nov 19	Hα	~1.4[b]	<500	<500	~1.2	[c]	[c]
Dec 28	Hα	~11.5[b]	650 ± 50	660 ± 50	~1.3	1.51 ± 0.03	[c]
1979 Feb 2.....	Hα	6.1	260 ± 30	[c]	[c]	[c]	[c]
Nov 25.....	Hβ	4.7	260 ± 20	270 ± 20	3.6	1.34 ± 0.02	1.16 ± 0.02
Nov 28.....	Hβ	7.4	260 ± 20	260 ± 20	2.3	1.50 ± 0.02	1.52 ± 0.02
1980 Dec 14	Hβ	14.8	640 ± 220	[c]	3.3	1.40 ± 0.07	1.20 ± 0.07
1981 Jan 8	Hβ	10.6:	580 ± 130	[c]	[c]	1.5:	1.2:
Feb 24.....	Hβ	5.2	230 ± 20	260 ± 20	1.8	1.60 ± 0.02	1.47 ± 0.02

[a] Used maximum value after second contact.
[b] Mean EW in totality.
[c] Unable to determine.

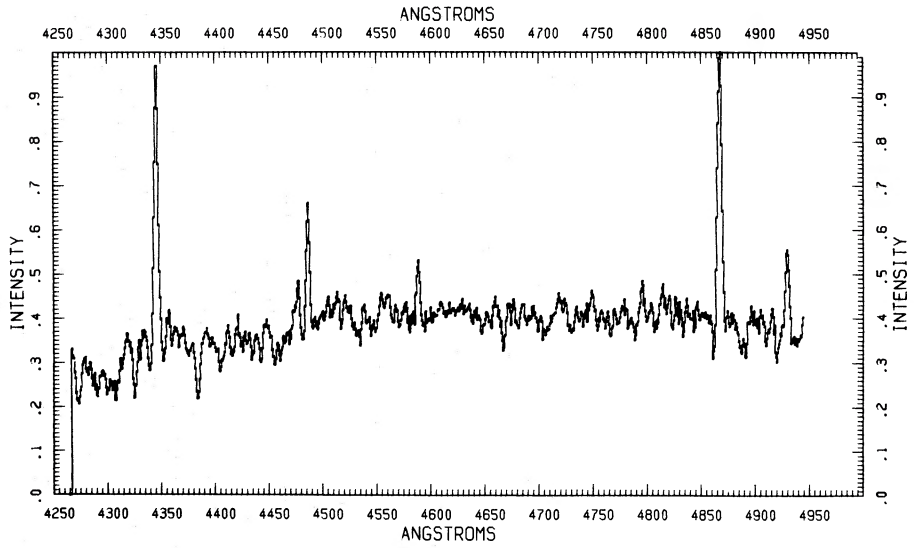

FIG. 1.—The spectrum of RW Tauri near second contact on 1979 Nov 28

and Plavec (1968). Plavec's (1968) estimate is based on the assumption that the line width is due to motion in a Keplerian disk. The error of this assumption will be seen below. The values listed in Table 2 show that the leading and trailing radii are seldom equal. Although the disk is noncircular, we will continue to use the term radius in the remainder of this paper because of its extensive use in the past.

To some extent it can be argued that the disk radius is actually set by the detection limit of the emission lines and a very tenuous disk may extend to a much larger radius. However, plots of line strength versus phase (see Figs. 3, 4, and 5) do imply a definite edge since the line strengths do not appear to asymptotically approach zero. A smooth extrapolation through the data points reaches zero line strength very near the last detection of emission. It is therefore likely that the radii in Table 2 represent the outer radius of at least the ionized gas.

The data of the three eclipses observed at KNPO are clearly superior to those observed at Link Observatory, principally because of the larger telescope aperture. For this reason, most of the remaining discussion will be based on the Kitt Peak eclipses, and in particular, on the eclipse of 1979 November 28. Figure 1 shows a spectrum taken near second contact on that night. Table 3 lists relative strengths of the emission lines visible at the three KPNO eclipses and the integrated Hβ flux. The strength of Hβ varied by almost a factor of 2 among eclipses, yet the relative line strengths remained nearly unaffected.

Figure 2 shows isometric plots of the Hβ emission line

TABLE 3

LINE STRENGTHS[a] AT SECOND CONTACT (Hβ = 1.0) KPNO ECLIPSES

Line	1979 Nov 25	1979 Nov 28	1981 Feb 24
Hγ (λ4340)	0.94 ± 0.05	0.93 ± 0.07	1.14 ± 0.04
He I(λ4471)	0.04 ± 0.03	0.07 ± 0.05	0.11 ± 0.01
Mg II(λ4481)	0.33 ± 0.05	0.32 ± 0.02	0.36 ± 0.01
Fe II(λ4584)	0.11 ± 0.02	0.13 ± 0.01	0.14 ± 0.02
Hβ(λ4861)	1.00	1.00	1.00
He I(λ4922)[b]	0.22 ± 0.05	0.25 ± 0.04	0.26 ± 0.05
Hβ flux (ergs s^{-1} cm^{-2})	2.76(±0.16) × 10^{-13}	5.11(±0.12) × 10^{-13})	3.81(±0.08) × 10^{-13}
Hβ flux[c] (ergs s^{-1} cm^{-2})	4.54(±0.26) × 10^{-13}	8.40(±0.02) × 10^{-13}	6.27(±0.13) × 10^{-13}

[a] Corrected for interstellar reddening using $A_v = 0.45$ and the Whitford (1958) reddening curve.

[b] There is a possibility that He I(λ4922) is blended with Fe II(λ4924). Some support for this is seen in the radial velocity of He I(λ4922) which is somewhat larger than the other lines at second contact.

[c] Corrected for interstellar absorption using $R = 3.0$.

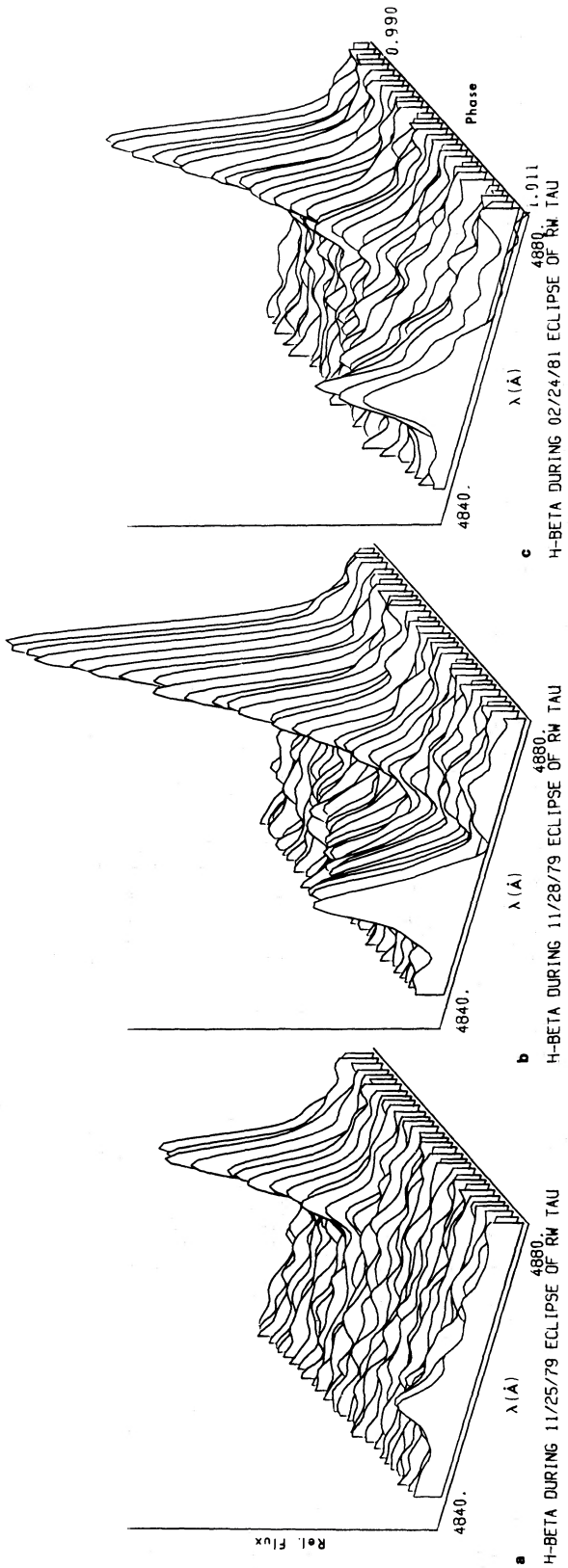

FIG. 2.—(*a*) An isometric plot of the *Hβ* region during totality on 1979 Nov 25. The vertical axis is a relative flux scale. The other two axes are orbital phase and wavelength in Angstroms. (*b*) The same plot as (*a*) for 1979 Nov 28. (*c*) The same plot as (*a*) for 1981 Feb 24.

during totality of these three eclipses, clearly showing the two Doppler components. The 1979 November eclipses are separated in time by only one orbit, yet the changes are quite strong. On 25 November the disk was completely eclipsed for about 20 minutes. However, one orbit later (November 28) the disk had grown to such an extent that the disk eclipse was partial. The 1981 February 24 eclipse was also partial.

In order to determine accurately emission-line profiles and radial velocities, it was necessary to correct for the very complex underlying absorption-line spectrum of the K-type secondary star. The 20 minute interval during the 1979 November 25 eclipse when the disk emission was absent contains the "pure" K star spectrum. Nine spectra in this interval were averaged and then subtracted from each spectrum in totality. The data in Figure 2 have been corrected in this manner.

To determine the line strengths, widths, and radial velocities, each emission line was fitted with a Gaussian profile, which gave an extremely good match to the observed lines. Figure 3 shows the parameters from the Hβ fitting for the November 25 eclipse. The vertical dotted lines mark the beginning and end of totality. During the partial phases the B star spectrum varies so rapidly in both flux and absorption-line profiles that corrections for its contribution to the measured quantities are very uncertain. Therefore, the data presented do not include the partial phases even though the disk emission lines can often be detected. The upper panel shows the behavior of the radial velocity, corrected to the center of mass of the system, versus phase. The systemic velocity was taken from Hiltner and Hardie (1949). The filled circles refer to the redshifted emission component and the open circles to the blueshifted components. The middle panel shows the full width at half-maximum (FWHM), corrected for the instrumental resolution. The bottom panel shows the integrated line flux. Note that the redshifted component is much stronger than the blueshifted component. The disk eclipse is total as indicated by a lack of data points between phases 0.0 and 0.005. The midpoint of the disk eclipse is not centered at phase 0.0 due to the unequal sizes of the disk on the leading and trailing side of the primary star.

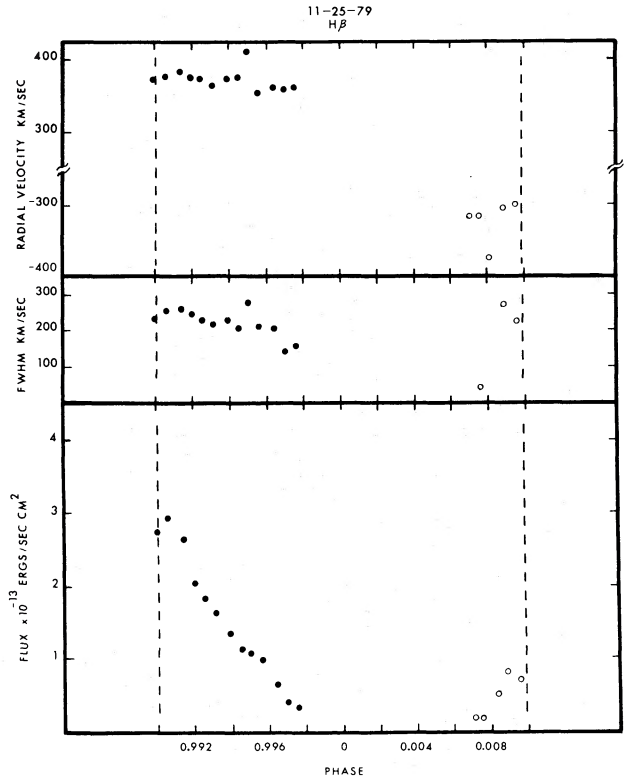

FIG. 3.—The integrated line flux, FWHM, and radial velocity for Hβ on 1979 Nov 25. The vertical dashed lines mark the beginning and end of totality. Filled circles refer to the redshifted component, and open circles refer to the blueshifted component. The observational error can be estimated from the scatter in the data points.

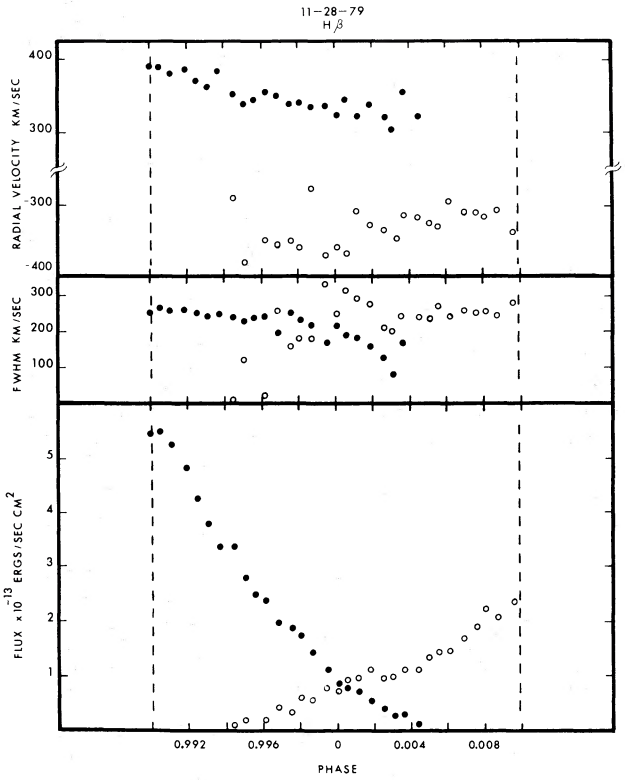

FIG. 4.—The same plot as Fig. 3 for 1979 Nov 28

Figure 4 displays the same information for the November 28 eclipse, one orbit later. As before, the redshifted component is brighter than the blueshifted component, but by a smaller margin. The disk eclipse is partial with both Doppler components simultaneously visible near mid-eclipse. The radial velocity behavior of the redshifted component at first appears consistent with a Keplerian disk. After second contact, the radial velocity decreases steadily as the inner regions of the disk are occulted. However, the velocity of the blueshifted component should become more negative from t_b until third

contact, as more of the inner disk comes into view. Instead, Figure 4 shows the opposite behavior. This is also clearly seen in the Hγ line; however, the blueshifted components of the other atomic species are too weak for a radial velocity study.

Figure 5 shows the emission-line behavior during the 1981 February 24 eclipse. Most of the comments made about the two previous eclipses are true for this one as well. The radial velocity behavior of the blueshifted component is difficult to characterize because of the scatter in the data. In any case, it does not appear to give strong support to a Keplerian velocity field. Near mid-eclipse the Hβ profiles showed a definite three-component structure. The third emission component was found near rest wavelength and could only be measured when the two disk components were weak. The squares in the bottom panel of Figure 5 indicate its approximate strength. This third component was much harder to detect in the Hγ profiles, indicating a steeper Balmer decrement than that of the disk. This, combined with the near constancy of its strength in eclipse, implies this emission comes from an extended, low-density region. A large circumstellar or circumsystem shell is thus indicated. The presence of a third emission component may explain some of the large line widths in Table 2. This emission component would not have been resolved in the spectra obtained at Link Observatory. However, this will not explain the line width problem to be described below.

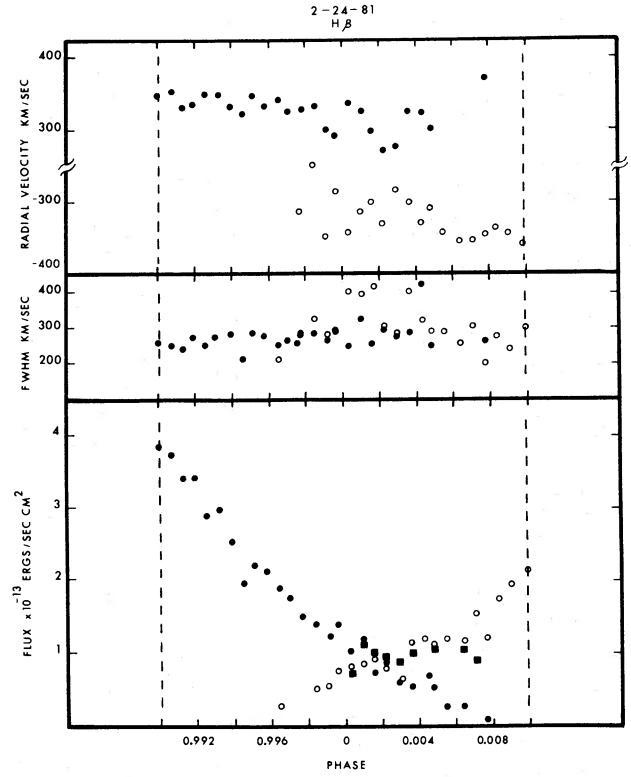

FIG. 5.—The same plot as Fig. 3 for 1981 Feb 24

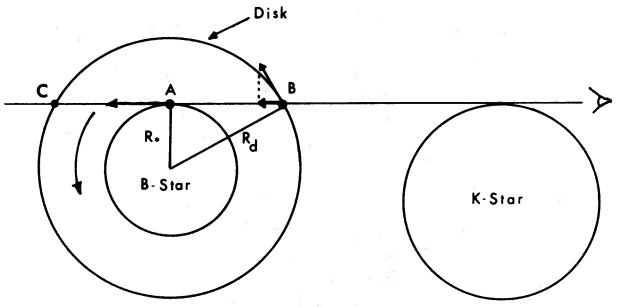

FIG. 6.—The disk geometry at second contact

a) The Velocity Field and Line Width Problem

For a thin disk whose rotational velocity decreases monotonically with radius, the total emission line width seen at second contact is determined by the disk velocity at the stellar surface and at the outer edge. Figure 6 shows the geometry at second contact (which is simplified by the system inclination being nearly 90°). The highest observed radial velocity originates at point A, while the lowest is the vector component of the velocity at the disk edge at point B. If the velocity field is assumed to be Keplerian and the stellar mass and radius are taken from Grant (1959) to compute the disk velocity at the star's surface, then the observed line width can be used to compute the radius of the disk. Plavec (1968) applied this technique to a spectrogram of Joy's to obtain a disk radius for RW Tauri of 2.61 R_*, which is much larger than any value in Table 2. This same technique applied to the eclipse of 1979 November 28 yields a radius of 4.9 R_* even though it was *measured* to be 1.51 R_*. Clearly some crucial assumption fails. The expected FWHM for a Keplerian disk with a radius of 1.5 R_* is about 100 km s^{-1}. Table 2 shows the emission lines are always at least a factor of 2 wider than this. An important asset of time-resolved spectroscopy is its ability to measure the disk's radius directly.

The remainder of this discussion is mostly limited to the 1979 November 28 eclipse which is the highest quality data set. Any features in substantial agreement or disagreement with other eclipses are noted. The velocity field on the leading side of the disk is clearly non-Keplerian, as seen by the radial velocity behavior in Figure 4. The velocity field on the trailing side is also non-Keplerian, as seen by a variety of indicators. At phase t_r only the very outer edge of the disk is visible, and the observed radial velocity corresponds to the rotational velocity. This velocity is 330 km s^{-1} (from Fig. 4) which is less than the expected Keplerian velocity by 50 km s^{-1}. This difference could be due to uncertainties in the mass of the primary star. However, as already indicated, the line widths are totally incompatible with a Keplerian field. At second contact the emission spans a velocity range from 65 to 690 km s^{-1}. If it is assumed that the velocity at the surface of the star is 690 km s^{-1}, then the velocity at the outer edge of a Keplerian disk of this size should be 561 km s^{-1} and not the observed 330 km s^{-1}.

The behavior of the redshifted emission-line radial velocity with phase for all observed eclipses implies that the rotational velocity field is a monotonically decreasing function of distance from the star. Yet such a field, Keplerian or otherwise, cannot explain the observed line widths. Such a field is required to have a value of 690 km s^{-1} at the stellar surface (to account for the high-velocity emission wing) and smoothly decrease to 330 km s^{-1} at the outer edge (to match the radial velocity at t_r). The lowest radial velocity will originate at point B in Figure 6, where the vector component of the 330 km s^{-1} rotational velocity along the line of sight is 220 km s^{-1} and not the 65 km s^{-1} required to account for the line width. Furthermore, such a velocity field would result in a rapid narrowing of the line after second contact as the inner, high-velocity regions are occulted. In fact, during all three KPNO eclipses, the line narrows very slowly with phase.

It is possible to obtain much wider lines if the disk is both rotating and infalling. For a monotonically decreasing rotational velocity field with infall, the geometry at second contact demands that the lowest observed radial velocities occur at point C in Figure 6. At this point the line-of-sight vector components of the rotation and infall are oppositely directed. To match the observed low velocity of 65 km s^{-1}, using 330 km s^{-1} as the rotational velocity at the disk edge requires an infall velocity of only 75 km s^{-1}. With such a small infall velocity the highest observed velocity of 690 km s^{-1} must still come from a region near point A in Figure 6. This leads to the same problem as before: the line should narrow rapidly after second contact.

The conclusions to be drawn are these. A simple rotational velocity field which monotonically decreases with distance must exist on the trailing side to account for the behavior of the radial velocity with phase. However, this field is non-Keplerian and cannot, even with infall, account for the observed line widths. There must be a strong line-broadening mechanism as well.

The observations provide some clues as to the nature of this broadening mechanism. For instance, the line widths are independent of the rotational velocity field. In Figure 4 it can be seen that the rotational velocity field is completely different on the leading and trailing sides of the disk. The rotational velocity decreases when moving toward the star over a significant portion of the leading side. Yet the line widths from both sides appear to be identical in every eclipse. Another clue is provided by the line profiles. The lines seen during all three KPNO eclipses appear to be nearly Gaussian. (Since the line width only exceeds the instrumental resolution by a factor of 2, it can only be said that the true profile is very symmetric. Numerical calculations showed that a small amount of asymmetry in the original line would have been detected.) These profiles also exclude a Keplerian disk as the sole determinant of line profile since such profiles would be quite asymmetric (Plavec 1968). Electron scattering is also excluded as a significant broadening mechanism due to the lack of scattering wings on the observed profiles.

The line-broadening mechanism apparently makes use of the Doppler effect. In all three KPNO eclipses the ratio of the line width to the rest wavelength was the same for Hγ and Hβ to within observational error. Furthermore, there appears to be a relationship between this ratio and atomic mass number, as seen in Figure 7. This same behavior is seen in the other two KPNO eclipses but, due to the larger error bars, it is less pronounced. This effect needs further confirmation. It appears to be real, but its exact form is difficult to characterize with the existing data. Figure 7 suggests thermal broadening of the lines, but this would require temperatures of 10^6–10^7 K and would therefore preclude the existence of the observed recombination-line spectrum. Another possible explanation is simply that the lines of heavier atomic species are formed in different locations of the disk which are less affected by the broadening mechanism. This explanation seems unlikely since, to within observational error, the emission-line "light curves" are the same shape for every atomic species. Therefore, no species has its emission arising from a region systematically closer to or farther from the star than any other species. This conclusion is limited to the trailing side of the disk since most lines on the leading side were too weak to make this comparison.

Possible explanations for the line-broadening mechanism appear to be few in number. The Doppler nature of the line widths and the symmetrical, perhaps Gaussian line profiles suggest turbulence as a possible mechanism. The star-stream interaction may be a source of turbulence. However, the required turbulent velocities would be 10–20 times the sound speed in the gas. There are three objections which immediately come to mind. First, supersonic turbulence would be expected to produce some shock fronts and high-excitation emission lines which have not been previously reported. Second, supersonic turbulence would be expected to dissipate rapidly. By the time the gas circulates from the leading

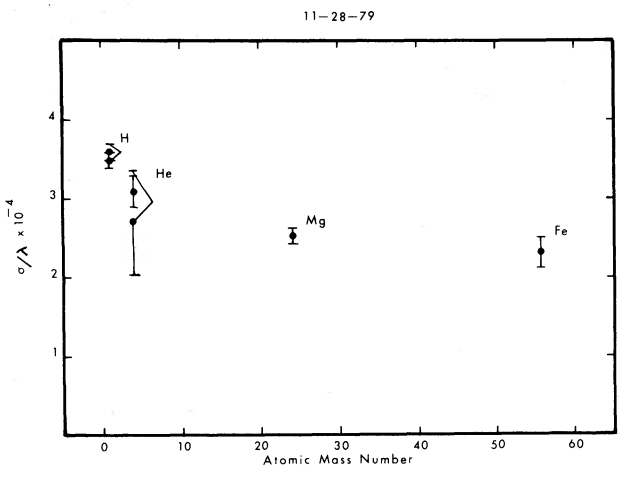

FIG. 7.—The line width versus atomic mass number for the 1979 Nov 28 eclipse. The line width is expressed as the ratio of the standard deviation of the Gaussian fit to the rest wavelength.

to the trailing side of the disk (about 5 hours), the emission lines should narrow. This is not observed, and the turbulence model would therefore require an energy source all the way around the disk. Finally, it is not clear how turbulence could result in line widths which depend on atomic mass.

In connection with the first objection, Plavec, Dobias, and Weiland (1982) recently found high-excitation emission lines in the ultraviolet spectrum of U Cephei. It may be that RW Tauri also has such lines. In addition, we report the first detection of He I emission in RW Tauri, which may be indicative of a hot plasma as it was for the W Serpentis stars (Plavec 1980).

It should be noted that a similar line width problem was encountered by Crawford (1981) for the Hα line seen during the 1974 and 1975 outburst of U Cephei (Plavec and Polidan 1975). He also suggested the possibility of supersonic turbulence as a line-broadening mechanism.

b) Physical Conditions in the Disk

It is clear from Table 3 that the ratio of Hγ to Hβ line strengths is near unity, which differs significantly from Menzel's case A or B (approximately 0.5). This departure is undoubtedly due to collisional effects which are important at the high densities anticipated in the disk. The most complete calculation to date of the Balmer decrement which includes collisional effects is that of Drake and Ulrich (1980). They treat a static slab of pure hydrogen with temperatures ranging from 5×10^3 to 4×10^4 K and electron densities from 10^8 to 10^{15} cm^{-3}. It is not possible to match uniquely the disk spectrum with any of their models since only two hydrogen lines were observed. However, their models do indicate, for a wide range of parameters, that a value of $n_e \geq 10^{13}$ cm^{-3} is required to produce the observed Hγ/Hβ ratio.

Figure 8 shows the behavior of the Hγ/Hβ ratio during totality of the 1979 November 28 eclipse. The difference between the leading and trailing sides of the disk is quite striking. On the trailing side the ratio remains high all the way out to the outer edge of the disk. On the leading side the ratio is high only when the inner regions are visible and drops to the value expected from Menzel's case B at the outer edge. Apparently, the gas density on the trailing side remains fairly high all the way out to the edge, while the density on the leading side drops rapidly with distance from the star. This behavior implies that, by the time the disk material has moved halfway around the star, the infall of gas has greatly depleted the outer disk regions.

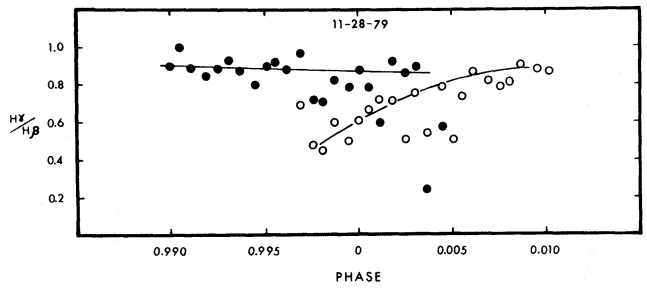

FIG. 8.—The Hγ/Hβ ratio versus phase during the 1979 Nov 28 eclipse. Filled circles refer to the redshifted component, and open circles refer to the blueshifted component. The lines are only guides to the eye. The ratio has been corrected for interstellar reddening.

The line profiles show no sign of a wing produced by electron scattering. This effect was used to estimate an upper limit to the mean electron number density. Line profiles were calculated as a function of electron scattering optical depth, τ_e, following the treatment of Castor, Smith, and Van Blerkom (1970). The width of the initial profile was chosen so that the final profile (after "smearing" by the instrumental profile) would have the same FWHM as the observed profile. This is a valid approximation since electron scattering predominantly affects the wings. A comparison of the calculated and observed profiles showed that $\tau_e \leq 0.1$. Since most of the line flux originates close to the star, the path length was taken as a chord passing through the disk of radius 1.5 R_* tangent to the star's equator. This yields a mean density, n_e,

$$n_e \leq 4 \times 10^{11} \text{ cm}^{-3},$$

which differs by a factor of 100 from the limit based on the Drake and Ulrich (1980) models. However, their model grid was necessarily limited, and it is possible that the line ratio could be matched at a lower density with the correct set of parameters. Their models are for a static atmosphere, and it is not clear how the rotational velocity field coupled with the line-broadening mechanism affects radiative transfer and the observed line ratio.

If collisional effects play an important role in determining line ratios, then they might enforce local thermodynamic equilibrium (LTE). The LTE assumption is most likely to be valid on the trailing side of the disk where collisional effects keep the Hγ/Hβ ratio large all the way to the disk edge. As previously mentioned, the emission-line light curve of each atomic species has the same shape as that of hydrogen. This means that the relative populations of all atomic levels remain the same and the trailing side of the disk is nearly isothermal. Thus, the emission-line intensity seen at second contact can be approximated by using a single Planck function and a mean optical depth. Since the optical depth in Hγ and Hβ are related by atomic constants, the Hγ/Hβ line ratio can be calculated as a function of temperature and of the Hγ optical depth. To obtain a unique solution, the He I(λ4471)/He I(λ4922) ratio was also calculated (assuming He I λ4922 is unblended with Fe II λ4924) for the same temperature and Hγ optical depth. The He line optical depths are related to the Hγ optical depth by atomic constants and the usual assumption of cosmic abundance. While it was possible to find many temperatures and optical depth combinations which produced the observed Hγ/Hβ ratio, no solution simultaneously satisfied both the hydrogen and helium line ratios. Apparently, either He I

λ4922 is blended or the physical conditions in the disk are such that collisional processes play an important role but do not dominate totally the spontaneous transitions in determining the populations of the atomic levels.

There are two curious observations about the trailing side of the disk which may be related. It seems rather strange that the density, as implied by the Hγ/Hβ ratio, should remain high to the outer edge where the disk ends abruptly. It also seems curious that the disk radius on the trailing side does not vary much from eclipse to eclipse. One possible explanation for both features is that the radius seen on the trailing side is not in fact the limiting radius but rather marks the ionization limit in the gas. To check the feasibility of this, a set of calculations was made to see if the B8 primary star could have an ionization radius of 1.5 R_* with a gas density and volume expected for the disk. The usual "Strömgren sphere" condition was assumed, namely that the number of ionizing photons entering the emitting volume each second is exactly balanced by the number of recombinations. Only photoionizations from the ground state were considered. The disk was assumed to have a cylindrical shape of constant thickness. It was further assumed that any ultraviolet photon which intersected the disk at any point produced an ionization. If the total thickness was set equal to the diameter of the B star as an upper limit, the mean electron density was found to be 1.0×10^{11} cm^{-3}. This result is in substantial agreement with the density estimate made earlier and gives support to the idea that the trailing side of the disk is radiation bound.

III. DISCUSSION

To extract the radial dependence of the physical conditions, such as temperature and density, requires some treatment of radiative transfer. Unfortunately, this cannot be done because of the unknown nature of the line-broadening mechanism. However, the observations do hold some clues as to the behavior of the rotational velocity, line width, and surface brightness of the disk as a function of distance from the central star. For example, as the leading edge of the disk emerges from eclipse, each succeeding spectrum changes because of the contribution of each newly visible disk "slice" at the limb of the K star. The rate at which the emission line brightens between each spectrum gives the flux contribution of each slice. Similarly, the observations contain information about the line width and radial velocity contribution of each slice. These statements are also true for the trailing side of the disk, with events occurring in reverse chronological order. It is therefore possible to obtain the run of these parameters across the visible surface of the disk. This is not the same as the functional dependence with distance from the star, but rather a mean over the emitting volume of each slice across the face of the disk. This at least gives some clues as to the true radial dependence of the parameters.

The technique used requires polynomial fitting of the data in Figure 4. These fits are not the only curves which can represent the data to within observational error. It is also difficult to assign error estimates to the results. For these reasons the results given below should be viewed as only a rough guide to the behavior of these parameters. No conclusions have been drawn from this analysis unless they could be justified by an inspection of the observational data.

In this procedure it was assumed that the emission profile from each slice could be approximated as a Gaussian function. The central wavelength of a slice, λ_s, was computed by assuming that the central wavelength of the emission line in the $i + 1$ spectrum is an average of the previous ith spectrum and the slice, weighted by their flux contributions, i.e.,

$$F_{i+1}\lambda_{i+1} = F_i\lambda_i + (F_{i+1} - F_i)\lambda_s .$$

The polynomial fits were used to obtain a smooth run of flux and wavelength. The value λ_s was found for all pairs of spectra in eclipse. The surface brightness distribution was found by differentiating the polynomial function for the flux with respect to distance from the central star. This is a potentially misleading surface brightness as it does not account for variations in disk thickness. Finally, the line width of each slice was approximated by the width of the profile produced by the subtraction of two Gaussians representing the emission lines in two successive spectrograms. The width, central wavelength, and amplitude of each Gaussian was taken from the polynomial fits to the observations.

Figure 9 shows the results for the Hβ line from the observations of 1979 November 28. The surface brightness on the trailing side drops rapidly with distance from the star. This behavior could be due to three effects. First, the line source function could be declining with distance. Second, the optical depth in the line could be changing, or third, the disk thickness could be decreasing. It has already been argued from the line ratios that the trailing side is nearly isothermal with almost constant density and the length of a chord through the disk along the line of sight decreases quite slowly immediately after second contact. These considerations strongly suggest that both the source function and optical depth should be slowly varying functions across the face of the disk. The variations seen in Figure 9 must then be due in large part to a disk of decreasing thickness with distance from the star. An isothermal disk in hydrostatic equilibrium in the direction perpendicular to the orbital plane will have a thickness which *increases* in proportion to $r^{3/2}$ (Shakura and Sunyaev 1973). Clearly, the observations imply the disk is not in hydrostatic equilibrium.

Further evidence of this is seen in the brightness distribution from the leading side. The Hγ/Hβ ratio suggests that the density close to the star is the same on both sides of the disk. The temperature and optical depths would also be expected to be the same. However, Figure 9 indicates a factor of 2 difference between the surface brightnesses of the two sides. The simplest way to account for this is with a factor of 2 decrease in thickness. Apparently, the disk has undergone collapse to the orbital plane in the approximately 5 hours

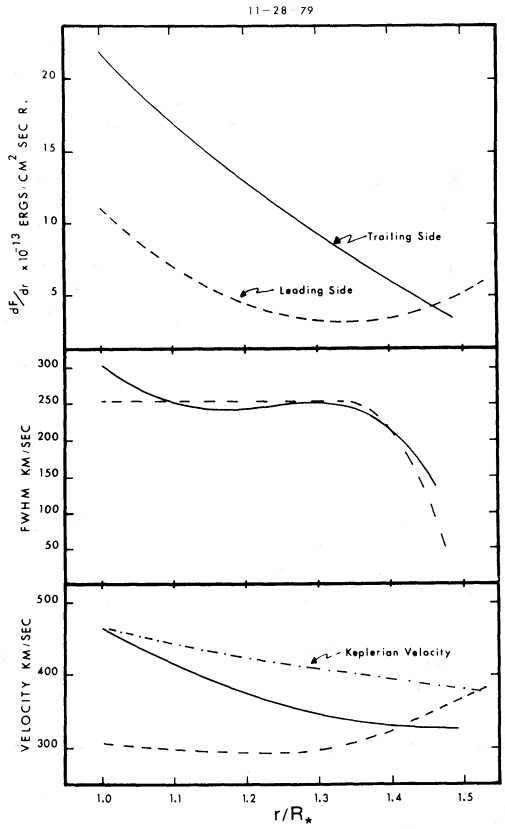

FIG. 9.—The surface brightness, line width, and radial velocity versus radius derived from the slice technique described in the text.

required for the gas to rotate halfway around the star. This picture is consistent with the expected time scale for collapse to the plane calculated from the typical disk radius, rotational velocity, and mass of the primary star.

Figure 9 shows that the surface brightness of the leading side decreases with distance from the star, reaches a minimum at 1.32 R_*, and then brightens toward the edge. The origin of this behavior can be seen in both Figures 4 and 5. As the leading side of the disk emerges from eclipse, the line flux increases. At about phase 0.001 it becomes nearly constant until phase 0.005, after which it brightens rapidly. Apparently, between these two phases, the disk portions coming into view are faint and contribute little to the total light of the disk. Note that the trailing side shows no such effect in Figures 9 or 4. A constant density and temperature approximation cannot be made for the leading side, as seen by the large variations of the Hγ/Hβ ratio. Thus, this surface brightness minimum could be due to either a reduced disk thickness or a variation in physical conditions.

The line width behavior is essentially identical on both sides of the disk, remaining nearly constant almost to the outer edge. Beyond a radius of 1.35 R_* the line width decreases rapidly. (The small upturn in the line width within 1.1 R_* on the trailing side is an artifact of the polynomial fitting.) The decreasing line width at the edge of the trailing side is not consistent with our earlier suggestion that this edge was actually an ionization limit. It seems unlikely that the line width should be affected by the location of the ionization limit.

The radial velocity behavior in Figure 9 is very different for the two sides of the disk. On the trailing side the velocity declines from 465 km s^{-1} at the surface of the star to 327 km s^{-1} at the outer edge. The velocity near the stellar surface is almost exactly the expected Keplerian velocity. However, it decreases much faster with distance than a Keplerian field in a manner very similar to that found by Crawford (1981) for the disk in U Cephei. The velocity behavior of the leading side is unusual, as would be expected from Figure 4. At the outer edge the velocity is nearly Keplerian (380 km s^{-1}) and then declines until a radius of 1.3 R_* which is approximately the same radius as the surface brightness minimum. From this point all the way to the stellar surface, the velocity is approximately constant. Apparently, in the few hours required for the gas to circulate around the star, the inner regions have slowed while the outermost regions have gained velocity.

IV. SUMMARY

From the above discussion we can summarize a fragmentary picture of the disk structure. The trailing side of the disk is a region of nearly constant density ($\sim 10^{11}$ cm^{-3}) and temperature whose thickness tapers toward the edge. It may be that the optical depth to stellar ultraviolet photons is so high that only the inner regions are ionized. Apparently, the star-stream interaction which produces the disk divides the free-fall energy of the stream between rotational and some random-like motion which greatly broadens the emission lines. The rotational velocities are below the Keplerian velocity, resulting in an infall of gas. There is also a collapse toward the orbital plane. By the time the gas has circulated to the leading side of the star, the disk thickness has been reduced by a factor of 2 and the infall has depleted the outer regions, causing an accumulation of gas near the stellar equator. There may be a density or thickness minimum about three-fourths out from the stellar surface. Finally, the rotational velocity field has been restructured with the highest velocities at the outer leading edge, at speeds approaching the Keplerian velocity.

One of the most important gaps in this picture is the unknown size and location of the region responsible for the optically thick continuum emission. This emission is especially strong at second and third contact and prevents the total phase of eclipse from being flat-bottomed. This effect has been studied in U Cephei by Olson (1980*b*), who finds the spectrum of this excess light is best matched by a model atmosphere of approximately the same temperature as the primary star. He has suggested this light is due to a penetration of the star by the gas stream, producing an equatorial bulge (Olson 1980*c*). If this bulge occurs in RW Tauri, then the geometrical models of the disk are greatly complicated. The emission lines may in fact originate

from a corona-like region surrounding the bulge. In addition to time-resolved spectroscopy, simultaneous multiband photometry or low-resolution spectral photometry is required to define the spatial relationship between the line and continuum emission regions. This observation would be an important step toward a more realistic model of the disk structure.

There are other indications that the disk structure may be far from simple. Just prior to third contact of the 1979 November 28 eclipse, sharp hydrogen absorption lines appeared near rest wavelength. These absorption features were not visible at the same phase just one orbit earlier. Their presence suggests an accumulation of matter near the trailing hemisphere of the secondary star. During the 1978 February 7 eclipse, the emission lines continued to brighten after second contact and reached a peak at phase 0.996. This too is difficult to explain with any simple geometry.

Probably the most perplexing question raised by this study concerns the nature of the line-broadening mechanism. Future observations should attempt to confirm the intriguing relationship between line width and atomic mass. Observations at higher spectral resolution are needed to see if the line profiles are indeed Gaussian or some more complex structure. Finally, it is important to point out again that, in at least this one interacting binary, there exists a strong line-broadening mechanism other than orbital disk motions. One should therefore exercise caution in deriving stellar masses by assuming that the emission line widths in disks arise only from Keplerian rotation. This technique is sometimes applied to cataclysmic variables to calculate the mass of the white dwarf. From other work in progress we also conclude that broadening, other than rotational broadening in a disk, contributes to the emission-line widths in at least one cataclysmic variable.

We would like to thank Edward C. Olson for sharing his photometry, Jeannette Barnes for her help with the I-IDS data reduction, Martin S. Burkhead for making some photometric observations, and Michelle Kaitchuck for many hours of assistance at Link Observatory. We would like to acknowledge the many helpful comments and suggestions made by Mirek Plavec and Thomas Mullikin. This work was partially supported by NSF grant AST 81-08712.

REFERENCES

Batten, A. H. 1973, *Binary and Multiple Systems of Stars* (New York: Pergamon), p. 179.
Bookmyer, B. B. 1977, *Pub. A.S.P.*, **89**, 533.
Castor, J. I., Smith, L. F., and Van Blerkom, D. 1970, *Ap. J.*, **159**, 1119.
Crawford, R. C. 1981, Ph.D. thesis, University of California, Los Angeles.
Drake, S. A., and Ulrich, R. K. 1980, *Ap. J. Suppl.*, **42**, 351.
Frieboes-Conde, H., and Herczeg, T. 1973, *Astr. Ap. Suppl.*, **12**, 1.
Grant, G. 1959, *Ap. J.*, **129**, 62.
Hiltner, W. A., and Hardie, R. H. 1949, *Ap. J.*, **110**, 438.
Joy, A. H. 1942, *Pub. A.S.P.*, **54**, 35.
———. 1947, *Pub. A.S.P.*, **59**, 171.
Lubow, S. H., and Shu, F. H. 1975, *Ap. J.*, **198**, 383.
Olson, E. C. 1980*a*, *Inf. Bull. Var. Stars*, No. 1839.
———. 1980*b*, *Ap. J.*, **237**, 496.
———. 1980*c*, *Ap. J.*, **241**, 257.
Plavec, M. 1968, *Bull. Astr. Inst. Czechoslovakia*, **19**, 11.
Plavec, M. J. 1980, in *IAU Symposium 88, Close Binary Stars: Observations and Interpretations*, ed. M. J. Plavec, D. M. Popper, and R. K. Ulrich (Dordrecht: Reidel), p. 251.
Plavec, M., and Polidan, R. S. 1975, *Nature*, **253**, 174.
Plavec, M. J., Dobias, J., and Weiland, J. 1982, *Bull. AAS*, **13**, 802.
Shakura, N. I., and Sunyaev, R. A. 1973, *Astr. Ap.*, **24**, 337.
Whitford, A. E. 1958, *A.J.*, **63**, 201.
Wyse, A. B. 1934, *Lick Obs. Bull.*, No. 464.

R. Kent Honeycutt and Ronald H. Kaitchuck: Astronomy Department, Indiana University, Bloomington, IN 47405